

See discussions, stats, and author profiles for this publication at: <https://www.researchgate.net/publication/346141326>

# Morphological and optical properties of $\alpha$ - and $\beta$ -phase zinc (II) phthalocyanine thin films for application to organic photovoltaic cells

Article in *The Journal of Chemical Physics* · October 2020

DOI: 10.1063/5.0022262

---

CITATIONS

15

READS

182

7 authors, including:



Jean-Pierre Bucher

University of Strasbourg

143 PUBLICATIONS 6,209 CITATIONS

[SEE PROFILE](#)



Jun Onoe

Nagoya University

185 PUBLICATIONS 2,406 CITATIONS

[SEE PROFILE](#)

# Morphological and optical properties of $\alpha$ - and $\beta$ -phase zinc ( $\text{II}$ ) phthalocyanine thin films for application to organic photovoltaic cells

Cite as: J. Chem. Phys. **153**, 144704 (2020); <https://doi.org/10.1063/5.0022262>

Submitted: 19 July 2020 . Accepted: 13 September 2020 . Published Online: 08 October 2020

Masahiro Kato, Masato Nakaya , Yuki Matoba, Shinta Watanabe , Koichi Okamoto , Jean-Pierre Bucher , and Jun Onoe 



View Online



Export Citation



CrossMark



## Your Qubits. Measured.

Meet the next generation of quantum analyzers

- Readout for up to 64 qubits
- Operation at up to 8.5 GHz, mixer-calibration-free
- Signal optimization with minimal latency

[Find out more](#)

 **Zurich**  
**Instruments**

# Morphological and optical properties of $\alpha$ - and $\beta$ -phase zinc ( $\text{II}$ ) phthalocyanine thin films for application to organic photovoltaic cells

Cite as: J. Chem. Phys. 153, 144704 (2020); doi: 10.1063/5.0022262

Submitted: 19 July 2020 • Accepted: 13 September 2020 •

Published Online: 8 October 2020



Masahiro Kato,<sup>1</sup> Masato Nakaya,<sup>1</sup> Yuki Matoba,<sup>1</sup> Shinta Watanabe,<sup>1</sup> Koichi Okamoto,<sup>2</sup> Jean-Pierre Bucher,<sup>3</sup> and Jun Onoe<sup>1,a)</sup>

## AFFILIATIONS

<sup>1</sup> Department of Energy Science and Engineering, Nagoya University, Furo-cho, Chikusa-ku, Nagoya 464-8603, Japan

<sup>2</sup> Department of Physics and Electronics, Osaka Prefecture University, Gakuen-cho, Naka-ku, Sakai, Osaka 599-8531, Japan

<sup>3</sup> Université de Strasbourg and Institut de Physique et Chimie des Matériaux de Strasbourg (IPCMS), UMR 7504, 67034 Strasbourg, France

<sup>a)</sup> Author to whom correspondence should be addressed: [j-onoe@energy.nagoya-u.ac.jp](mailto:j-onoe@energy.nagoya-u.ac.jp). Tel./Fax: +81-52-789-3784

## ABSTRACT

We have investigated the morphological and optical properties of  $\alpha$ - and  $\beta$ -phase Zinc Phthalocyanine (ZnPc) thin films for application to organic photovoltaic cells (OPVs). It was found that the  $\alpha$ -phase is completely converted to the  $\beta$ -phase by thermal annealing at 220 °C under ultrahigh vacuum conditions. When the  $\alpha$ - to  $\beta$ -phase transition takes place, the surface roughness of the ZnPc film became flat uniformly with a nanometer order of unevenness by anisotropic growth of crystalline grains along a lateral direction to substrates. Correspondingly, the optical absorbance of the  $\beta$ -phase film became greater by 1.5–2 times than that of the  $\alpha$ -phase one in an ultraviolet-visible–near infrared (UV-vis-NIR) wavelength range, which plays a role in increasing the number of photogenerated excitons. On the contrary, time-resolved photoluminescence measurements showed that the average lifetime of excitons for the  $\beta$ -phase film became shorter by 1/6–1/7 than that for the  $\alpha$ -phase one, which plays a role in decreasing the number of excitons achieving the donor/acceptor interface where excitons are separated to carriers (holes and electrons). Both the increase in the number and the shortening in the average lifetime have a trade-off relationship with each other for contribution to the photoelectric conversion efficiency of OPVs. Then, we examined an external quantum efficiency (EQE) of OPVs using the  $\alpha$ - and  $\beta$ -phase films as a donor and obtained that the former OPV ( $\alpha$ -phase) exhibits a higher EQE by ~2 times than the latter one ( $\beta$ -phase) in the wavelength range of 400 nm–800 nm.

Published under license by AIP Publishing. <https://doi.org/10.1063/5.0022262>

## I. INTRODUCTION

High-performance photoelectric conversion devices have attracted a great deal of attention as one of the key technologies for the development of a sustainable society. Organic photovoltaic cells (OPVs) have been extensively investigated owing to their fascinating advantages of low weight, flexibility, highly designability, and reduced fabrication cost using inkjet printers when compared to conventional solar cells based on silicon (Si) and semiconductor compounds (SCs).<sup>1,2</sup> However, OPVs exhibit energy conversion efficiencies ( $\eta$ ) of ~10% at most,<sup>3</sup> which is still much lower than

those for the conventional Si ( $\eta_{\max}$ : ~25%) and SC ( $\eta_{\max}$ : ~40%) solar cells.<sup>4</sup> To further improve the  $\eta$  of OPVs, it is indispensable to essentially understand the mechanisms both of photoconversion current (short-circuit current) and open-circuit voltage using OPVs with well-defined structures.<sup>5</sup> For the former case, it is important to elucidate how structural and physicochemical properties of donor (D) and acceptor (A) molecular films affect the elemental processes: (i) photogenerated excitons in the D and A films, (ii) exciton diffusion to the D/A interface, (iii) separation of excitons to electrons and holes at the interface, and (iv) those carriers moving to electrodes, respectively.

In the present study, we focus on the elemental processes (i) and (ii) for OPVs with a heterojunction between Zinc Phthalocyanine (ZnPc) and fullerene ( $C_{60}$ ) thin films that are used as donor and acceptor, respectively. ZnPc/ $C_{60}$  OPVs have been widely investigated because the well-defined D/A heterojunction is suitable to understand the elemental processes of photoelectric conversion when compared to OPVs with a bulk-heterojunction.<sup>3,6–10</sup> In this system, since the molecular arrangement and domain structure of ZnPc films markedly depend on growth rate, deposition temperature, film thickness, and substrate (flatness, reactivity, etc.),<sup>11–16</sup> it is important to investigate how the structural features affect the optical properties (absorbance and dynamics) of the ZnPc film for improving the  $\eta$  of  $C_{60}$ /ZnPc OPVs. In fact, there have been many reports on the  $\eta$  and external quantum efficiency (EQE) of the ZnPc/ $C_{60}$  OPVs.<sup>17–21</sup> For examples, they investigated the influence of the indium-tin-oxide (ITO)/ZnPc interface on open-circuit voltage/recombination/cell degradation,<sup>17</sup> the influence of buffer layers on the exciton recombination or  $\eta$ ,<sup>18,20</sup> the influence of molecular orientation on photovoltaic properties,<sup>19</sup> and the structural influences on the charge carrier dynamics.<sup>21</sup> Thus, we here examined the structural (domain size, morphology, and roughness) and optical (absorbance and lifetime) properties of the  $\alpha$ - and  $\beta$ -phase ZnPc thin films, respectively, and compared the EQE between OPVs using the  $\alpha$ - and  $\beta$ -phase ZnPc films.

Figure 1 schematically illustrates the molecular structure of ZnPc (a), two types (brickstone and herringbone) of the metastable

$\alpha$ -phase ZnPc crystal structure (b), and the stable  $\beta$ -phase ZnPc crystal structure (c). For the latter phase, the monoclinic structure with two molecules per unit cell was confirmed,<sup>22</sup> whereas for the former phase, some morphs have been proposed.<sup>23</sup> Since the metastable polymorph  $\alpha$ -phase CuPc film has been reported that a herringbone arrangement was observed for a film thickness of 10 nm, whereas coexistence of both the herringbone and brickstone arrangements was found for a film thickness exceeding 10 nm,<sup>24</sup> we also consider these two arrangements for the metastable  $\alpha$ -phase ZnPc film as well in the present study, as shown in Fig. 1(b).

## II. EXPERIMENTS AND THEORETICAL CALCULATIONS

### A. Experiments

ZnPc films were formed in an ultrahigh vacuum (UHV) chamber (base pressure:  $2 \times 10^{-6}$  Pa) equipped with Fourier-transform infrared (FT-IR) spectrometer (JASCO, FT/IR-6600, resolution:  $0.5 \text{ cm}^{-1}$ ).<sup>25</sup> After thermal cleaning ( $260^\circ\text{C}$ ) of double-side polished  $\text{SiO}_2/\text{Si}(100)$  (Fig. 3) and quartz (Figs. 2 and 4–8) substrates, ZnPc molecules were deposited on these substrates at room temperature (RT) by thermal evaporation of ZnPc powders (purity: 98%) in a graphite crucible at  $285^\circ\text{C}$ . The growth rate was kept to be  $0.4 \text{ nm/min}$  for all films used here. The molecular orientation and domain structure of ZnPc films before and after thermal annealing were examined by *in situ* FT-IR spectroscopy at RT *in vacuo* and atomic force microscopy (AFM) with a dynamic force mode at RT in air, respectively. The crystal structure of the thermally annealed ZnPc film was also examined by x-ray diffraction (XRD) at RT in air. The optical absorbance of the ZnPc films thus formed was measured using a UV-vis-NIR spectrometer (JASCO V-630) with a resolution of  $0.5 \text{ nm}$  at RT in air. Photoluminescence (PL) spectra were recorded at RT in air using an apparatus consisting of a He-Cd laser ( $\lambda = 325 \text{ nm}$  and  $442 \text{ nm}$ ), a He-Ne laser ( $\lambda = 633 \text{ nm}$ ), a CCD camera (Princeton Instruments, PIXIS100), and a multi-channel

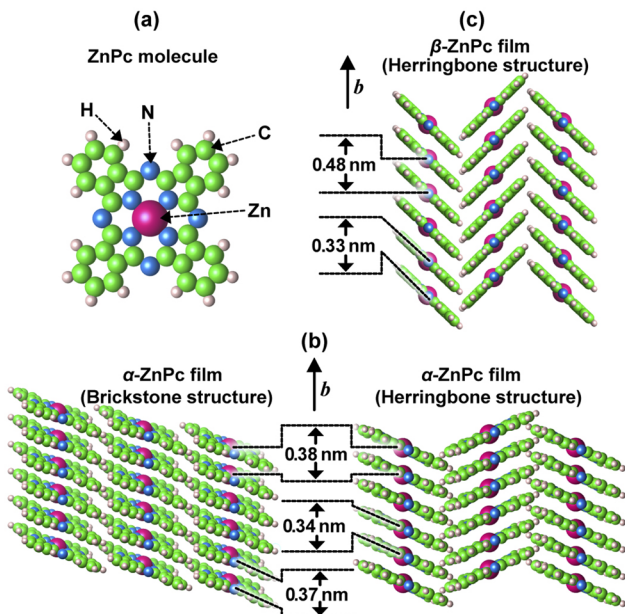


FIG. 1. Schematic illustration of ZnPc molecule (a), two types of the metastable  $\alpha$ -phase ZnPc crystal structure along  $b$ -axis (b), and the stable  $\beta$ -phase ZnPc crystal structure along  $b$ -axis (c). The Zn-Zn interatomic distance between adjacent ZnPc molecules is 0.38 nm and 0.48 nm for the  $\alpha$ - and  $\beta$ -phases, respectively. The intermolecular distance between them is 0.34 nm and 0.37 nm for the herringbone and brickstone structures of the  $\alpha$ -phase, whereas it is 0.33 nm for the herringbone structure of the  $\beta$ -phase.

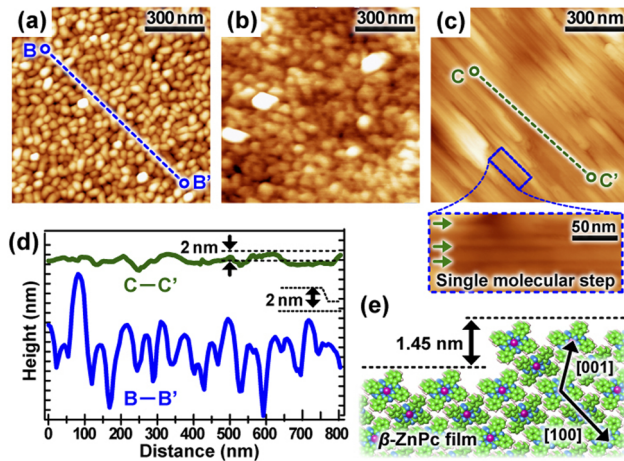


FIG. 2. AFM images of ZnPc films on quartz as deposition (a) and after annealing at (b)  $200^\circ\text{C}$  and at (c)  $220^\circ\text{C}$ . Blue and green lines (d) show the cross-sectional line profiles obtained along B-B' (a) and C-C' (c) line segments, respectively.

spectrometer (Roper Scientific, SpectraPro 2300i).<sup>26</sup> Time-resolved PL (TR-PL) were obtained at RT in air using a picosecond pulsed diode laser (Hamamatsu Photonics, PLP-10) as an excitation light source. The wavelength, pulse width, and repetition rate of the diode laser were set to 409 nm, 80 ps, and 10 kHz, respectively. A time-correlated single photon counter (PicoQuant, PicoHarp 300) was used to measure the PL time profile.

For fabrication of OPV cells, a 40 nm-thick  $\alpha$ - and/or  $\beta$ -phase ZnPc thin film was formed on 1 mm-wide 140 nm-thick indium-tin-oxide (ITO) substrates (Aldrich) in the UHV chamber. Thereafter, 30 nm-thick C<sub>60</sub> film was deposited on each ZnPc/ITO substrate at RT by thermal evaporation (400 °C) of C<sub>60</sub> powder (Matsubo Co. Ltd., 99.98% pure) in the same UHV chamber. Finally, 1 mm-wide 100 nm-thick aluminum (Al) (Nirako, 99.999% pure) cathode contact was formed on each C<sub>60</sub>/ZnPc/ITO substrate at RT by thermal evaporation in the other high vacuum chamber (base pressure: 10<sup>-4</sup> Pa). Thus, the active area of the present OPV cells was 1 mm<sup>2</sup>. The external quantum efficiency (EQE) of the OPV cells thus formed was recorded at RT in air by using a lock-in amplifier (Toyo Corporation 5210, modulation range: 400 Hz–450 Hz) in the range of 400 nm–800 nm.<sup>9</sup> By adjusting the incident angle of 90° normal to the cells, the device area of 1 mm<sup>2</sup> was irradiated with the parallel monochromatic light.

## B. Theoretical calculations

To estimate the polarization dependence of Q-band absorption spectra of the ZnPc monomer model for the  $\alpha$ - and  $\beta$ -phase ZnPc films, we calculated the oscillator strength of one-electron excitation states using the first-principles relativistic configuration-interaction (CI) method.<sup>27,28</sup> As the active space of CI calculations, 6 electrons and 14 molecular spinors were considered. The oscillator strength was evaluated using the general equation of the electric dipole transition between the initial and final states with the many-electron wavefunctions. The polarization dependence was estimated using the following three types of molecular orientation: the electromagnetic field of incident light ( $e$ ) is (i) perpendicular ( $e \perp D_{4h}$ ), (ii) inclined by 45°, and (iii) parallel ( $e \parallel D_{4h}$ ) to the D<sub>4h</sub> molecular axis of ZnPc. Since UV-vis-NIR absorption spectra of the ZnPc films have been understood in terms of the four-frontier orbital (HOMO – 1, HOMO, LUMO, and LUMO + 1) model proposed by Gouterman,<sup>29–31</sup> we also basically focused on these four orbitals.

## III. RESULTS AND DISCUSSION

Figure 2(a) shows the AFM image of the 100 nm-thick ZnPc film on the quartz substrate at RT. It is found that the film was composed of small granular grains with an average size of 40 nm, where no obvious crystalline facets were observed. As shown in Fig. 2(d), the cross-sectional line profile (blue line) obtained along the B–B' line segment in Fig. 2(a) indicates that the surface roughness of the ZnPc film was almost 20 nm–30 nm owing to their granular structures. As shown in Fig. 1(b), the metastable  $\alpha$ -phase is known to be formed preferentially (kinetically favorable) on substrates at RT.<sup>12–16,32</sup> After post-annealing at 200 °C for 60 min under UHV, Fig. 2(b) shows that the ZnPc film kept a high-dense granular structure with maintaining the  $\alpha$ -phase as discussed later (Fig. 3).

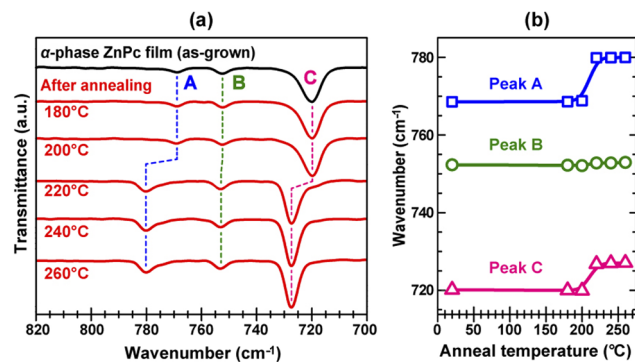


FIG. 3. (a) The evolution of FT-IR spectra with respect to annealing temperatures for the 100 nm-thick ZnPc film on the SiO<sub>2</sub>/Si(100) substrate. All spectra were measured *in situ* at RT under UHV. (b) Plot of the position for peaks A (blue), B (green), and C (pink) as a function of annealing temperatures.

On the other hand, Fig. 2(c) shows that the domain structure and surface roughness of the ZnPc film were drastically changed after post-annealing at 220 °C for 60 min. The cross-sectional line profile [green line of Fig. 2(d)] obtained along the C–C' line segment in Fig. 2(c) indicates that the molecularly flat domains with a surface roughness of ~2 nm were formed in a large area via no obvious formation of three-dimensional islands in association with desorption of ZnPc molecules, which was caused by an anisotropic growth of the  $\beta$ -phase domains [Fig. 2(c)] owing to thermal enhancement of planar stacking of ZnPc molecules. This finding is useful to fabricate a well-defined flat heterojunction of [electrode/C<sub>60</sub>/ZnPc/electrode] OPVs.

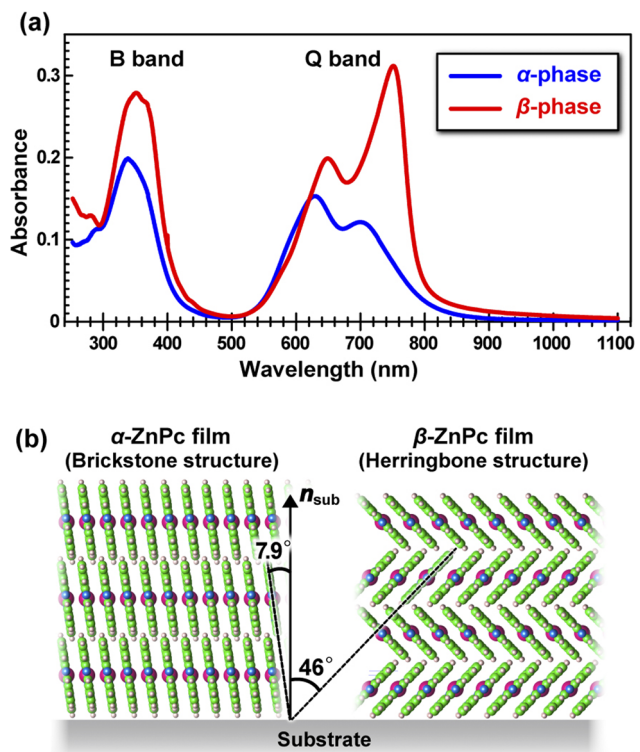
To understand the structural changes in the ZnPc film before and after post-annealing at 220 °C, we next examined temperature-evolution of FT-IR spectra for the 100 nm-thick ZnPc film deposited on the Si(100) substrate with a naturally native thin oxide layer. Since the three IR bands appearing between 700 cm<sup>-1</sup> and 800 cm<sup>-1</sup>, which are sensitive to crystal packing arrangements, are often used to differentiate between different polymorphs of ZnPc,<sup>33</sup> we focused on these IR bands. Figure 3 shows (a) *in situ* FT-IR spectra of the film after post-annealing at 180 °C, 200 °C, 220 °C, 240 °C, and 260 °C and (b) plot of their peak positions with respect to annealing temperatures in the wavenumber range. According to the previous first-principles calculations,<sup>33</sup> both peaks A and C were assigned to the out-of-plane mode of ZnPc molecule, whereas peak B was assigned to the in-plane mode. As shown in Fig. 3(b), it is found that peaks A and C were discontinuously shifted toward a higher wavenumber in temperatures between 200 °C and 220 °C, whereas peak B almost remained unchanged. Since peaks A and C are attributed to the out-of-plane motions, they are sensitive to the change in molecular orientation between adjacent ZnPc molecules. On the other hand, peak B originating from in-plane motions is not affected significantly by the orientational change. For the ZnPc films, the stable  $\beta$ -phase has been reported to be formed by post-annealing of the metastable  $\alpha$ -phase and/or by deposition of ZnPc molecules at high substrate temperatures,<sup>16,17,34–37</sup> which suggests that the IR spectral change after post-annealing at 220 °C was caused by the transition from the  $\alpha$ - to  $\beta$ -phase. As shown in Fig. 1(b), the  $\alpha$ -phase has the

brickstone and herringbone arrangements. Since peaks A and C are both assigned to the out-of-plane modes (see Fig. S3 in Ref. 33), their peak positions are significantly affected by the intermolecular distance between adjacent ZnPc molecules. When the  $\alpha$ - to  $\beta$ -phase transition takes place, the intermolecular distance changes from 0.37 nm to 0.33 nm for the brickstone arrangement, whereas from 0.34 nm to 0.33 nm for the herringbone arrangement, as shown in Fig. 1(b). Judging from the change in the intermolecular distance for the brickstone and herringbone arrangements after the phase transition, the discontinuous peak shift for both peaks A and C can be explained by assuming that the brickstone arrangement is dominate for the metastable  $\alpha$ -phase in the present study. Although the transition from the brickstone-type  $\alpha$ -phase to the  $\beta$ -phase will occur via the herringbone-type  $\alpha$ -phase as an intermediate, the drastic peak shift appearing in the annealing temperatures between 200 °C and 220 °C suggests that the herringbone-type  $\alpha$ -phase was formed and disappeared during the annealing at 220 °C for 60 min. It is found from the results in Figs. 2 and 3 that the grain size, morphology, and molecular arrangement changed simultaneously upon the phase transition at 220 °C.

We also confirm the  $\beta$ -phase film formed at 220 °C using XRD pattern showing a single diffraction peak at  $2\theta = 6.9^\circ$ , which is assigned to the diffraction due to  $(-101)$  planes of simple monoclinic (sm) for the  $\beta$ -phase ZnPc crystal.<sup>12,13,15</sup> This indicates that the ZnPc(-101)<sub>sm</sub> lateral to the quartz surface was formed after post-annealing at 220 °C [see Fig. 4(b)].

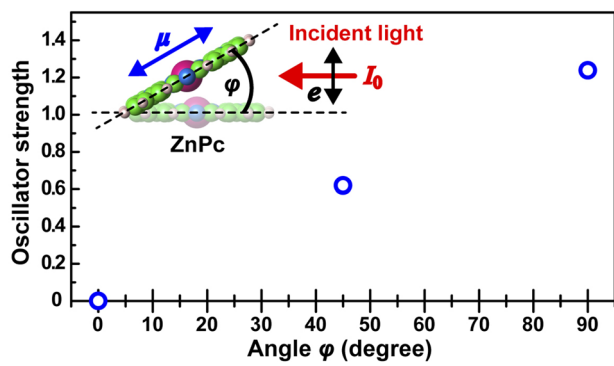
We next examined the changes in optical characteristics of ZnPc films before and after the phase transition. Figure 4 shows (a) UV-vis-NIR absorption spectra of the 100 nm-thick brickstone-type  $\alpha$ -phase (blue) and  $\beta$ -phase (red) ZnPc films formed on quartz substrates and (b) schematic illustration of the brickstone-type  $\alpha$ -phase and herringbone-type  $\beta$ -phase on the quartz substrates. Both spectra exhibited two intense absorption bands in the ranges of 300 nm–400 nm and 550 nm–800 nm, respectively. The former called the Soret (B) band originates from excitations between HOMO – 1 and LUMO/LUMO + 1, whereas the latter called the Q band originates from those between HOMO and LUMO/LUMO + 1.<sup>14,17,38–40</sup> Comparison of the spectra between the  $\alpha$ - and  $\beta$ -phase films indicates that the absorbance of both B and Q bands for the  $\beta$ -phase (red line) became greater by 1.5–2 times than those for the  $\alpha$ -phase film (blue line). This can be explained by changing the configuration between the molecular dipole moment of ZnPc molecule and the electric-field vector of incident light via the phase transition. We next examined the oscillator strength of ZnPc molecule under light irradiation using first-principles calculations.

Figure 5 shows the theoretical oscillator strength of ZnPc molecule as a function of the angle  $\varphi$  between the ZnPc molecule and the incident light. Here, the electric-field vector ( $e$ ) is orthogonal to the incident direction of light, whereas the dipole moment ( $\mu$ ) of the ZnPc molecule is also orthogonal to its  $D_{4h}$  molecular axis. Accordingly, since the  $\mu$  and  $e$  are orthogonal to each other at  $\varphi = 0$ , the oscillator strength becomes the minimum value of  $1.97 \times 10^{-6}$  (regarded as zero). On the other hand, since the  $\mu$  and  $e$  are parallel to each other at  $\varphi = 90^\circ$ , the oscillator strength becomes the maximum value of 1.24. In the present UV-vis-NIR measurements, the direction of the incident UV-vis-NIR light was parallel to the normal vector ( $n_{\text{sub}}$ ) of the substrate [see Fig. 4(b)]. Since the ZnPc



**FIG. 4.** (a) UV-vis-NIR spectra of the 100-nm thick  $\alpha$ -phase (blue) and  $\beta$ -phase (red) ZnPc films formed on quartz substrates and (b) schematic illustration for the crystal structure of the brickstone-type  $\alpha$ -phase (left) and herringbone-type  $\beta$ -phase (right) on the quartz substrates. Here, the  $n_{\text{sub}}$  denotes a vector normal to the substrate.

molecules of the  $\alpha$ -phase stand up with an angle of 9° to the  $n_{\text{sub}}$  [the left panel of Fig. 4(b)],<sup>35</sup> the angle between the  $\mu$  and  $e$  was estimated to be 81°, which gave rise to a small oscillator strength. In a similar manner, since the angle was estimated to be 46° for the  $\beta$ -phase, the



**FIG. 5.** Theoretical oscillator strength of the ZnPc molecule as a function of the angle  $\varphi$  between the ZnPc molecule and incident light. Here, the electric-field vector ( $e$ ) is orthogonal to the direction of the incident light, whereas the dipole moment ( $\mu$ ) of ZnPc is also orthogonal to its  $D_{4h}$  molecular axis.

oscillator strength became greater than that for the  $\alpha$ -phase. Thus, the absorbance of both B- and Q-bands for the  $\beta$ -phase (red) was greater than those for the  $\alpha$ -phase (blue), as shown in Fig. 4.

In general, an increase in the optical absorbance of both donor and acceptor films is expected to improve the photocurrent of OPVs because the number of photogenerated excitons is correspondingly increased. For example, Zhou *et al.* reported that the energy conversion efficiency of C<sub>60</sub>/ZnPc OPVs with a planer junction is increased by insertion of nanostructured copper iodide (CuI) layers between the transparent electrode and ZnPc film.<sup>41</sup> In this case, since a strong interaction between the surface electronic states of CuI and the molecular  $\pi$ -orbitals of ZnPc led to make ZnPc molecules laid down to substrate, the optical absorbance of ZnPc film became greater in a similar reason to the results in Fig. 4. Although the surface modification of electrodes has been a useful method to simultaneously control the molecular arrangement and the contact resistance at molecules/electrode interfaces,<sup>41,42</sup> an increase in the number of interfaces makes it difficult to understand the elementary processes (optical absorption, exciton generation/diffusion, and carrier conduction) for improving the photoelectric conversion of OPVs. Thus, we employed OPV cells with a well-defined structure in order to understand what influences the individual processes.<sup>43</sup>

We next examined photoluminescence (PL) spectra of the 100 nm-thick  $\alpha$ - and  $\beta$ -phase ZnPc films on quartz substrates in order to discuss a difference in the dynamics of photogenerated excitons between them. Figure 6 shows PL spectra of the  $\alpha$ -phase (blue) and  $\beta$ -phase (red) ZnPc films under irradiation with an excitation wavelength ( $\lambda_e$ ) of 325 nm (top), 425 nm (middle), and 633 nm (bottom). PL intensity of each spectrum was normalized using the power of each excitation light. The two PL peaks, L <sub>$\alpha$ 1</sub> (912 nm) and L <sub>$\alpha$ 2</sub> (968 nm), were observed for the  $\alpha$ -phase film, whereas two PL peaks, L <sub>$\beta$ 1</sub> (775 nm) and L <sub>$\beta$ 2</sub> (866 nm), were observed for the  $\beta$ -phase film,

except the excitation wavelength of  $\lambda_e = 425$  nm. These two PL peaks originate from S<sub>1</sub> to S<sub>0</sub> with two levels caused by the vibronic interactions (Jablonski diagram).<sup>43–46</sup> The very weak PL spectra (middle) obtained at  $\lambda_e = 425$  nm was due to the weak absorbance at 425 nm for both phases, as shown in Fig. 4. Comparison between the results in Figs. 4 and 6 indicates that the absorption and PL spectra of the  $\beta$ -phase film show a mirror image relationship in wavelength and intensity because the PL originates from  $\pi-\pi^*$  radiative relaxation via the Q band. For the  $\alpha$ -phase film, a large Stokes shift in the two PL peaks was observed when compared to its absorption spectra. This suggests that non-radiative relaxations of excitons should be considered for the  $\alpha$ -phase film. Correspondingly, the PL intensity of the  $\alpha$ -phase film drastically decreased at  $\lambda_e = 325$  nm when compared to that at  $\lambda_e = 633$  nm. This is because the non-radiative paths in the relaxation process increased in accordance with electron excitation to higher energy states. Thus, the non-radiative relaxation paths were drastically reduced by the thermal-induced phase transition from the  $\alpha$ - to  $\beta$ -phases.

In general, PL intensity for molecular assemblies (crystals and thin films) is markedly reduced by collision between excitons via non-radiative annihilation processes, the so-called concentration quenching. This quenching usually occurs for molecular assemblies with a well-ordered arrangement because the exciton diffusion coefficient is generally expected to become large for the assemblies. However, a remarkable decrease in the PL intensity was not observed for the  $\beta$ -phase film, despite that the size and ordering of domains in the ZnPc film became large and long, respectively, by the transition from the  $\alpha$ - to  $\beta$ -phase. This assumes that the lifetime of exciton would become shorter after the phase transition. To confirm this, we next evaluated an average lifetime ( $\tau_{avg}$ ) of excitons by examining time-resolved (TR) PL spectra of the  $\alpha$ - and  $\beta$ -phase ZnPc films.

Figure 7 shows TR-PL spectra of the 100 nm-thick  $\alpha$ - (blue) and  $\beta$ - (red) phase ZnPc films on quartz substrates. Here, the black lines denote fitting curves obtained using the time-variable equation based on two kinds of relaxation lifetimes, as expressed in the following equation:

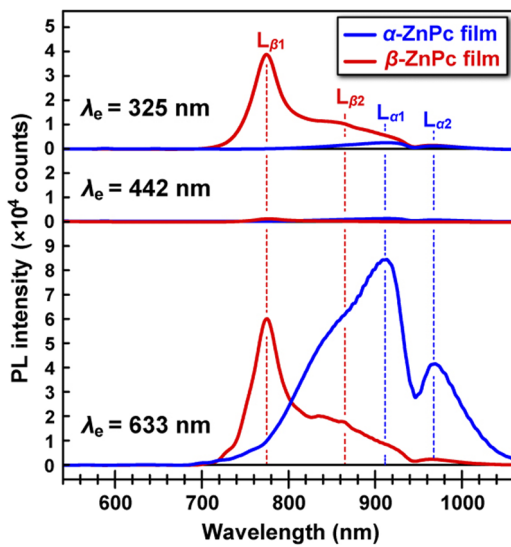


FIG. 6. PL spectra of the  $\alpha$ -phase (blue) and  $\beta$ -phase (red) ZnPc films on quartz substrates. Each spectrum was measured at an excitation wavelength of 325 nm (top), 425 nm (middle), and 633 nm (bottom), respectively.

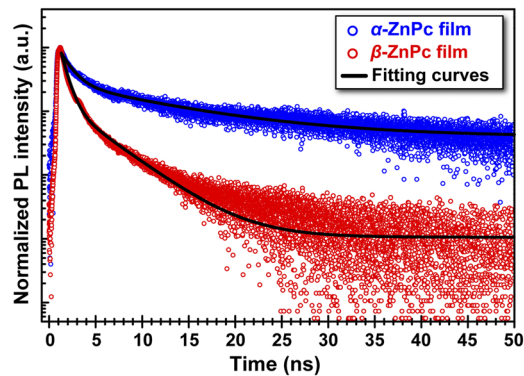


FIG. 7. Normalized TR-PL spectra of the  $\alpha$ -phase (blue circles) and  $\beta$ -phase (red circles) ZnPc films on quartz substrates. Black lines denote fitting curves for the experimental spectra.

$$I(t) = A_1 e^{-\frac{t}{\tau_1}} + A_2 e^{-\frac{t}{\tau_2}}, \quad (1)$$

$$\tau_{\text{avg}} = \frac{A_1 \tau_1 \tau_1 + A_2 \tau_2 \tau_2}{A_1 \tau_1 + A_2 \tau_2}. \quad (2)$$

Then, we estimated the  $\tau_{\text{avg}}$  for each phase film from the fitted values of coefficients ( $A_1$  and  $A_2$ ) and lifetimes ( $\tau_1$  and  $\tau_2$ ) using Eq. (2).

As shown in Fig. 7, the data deviation after 15 ns seemed to become wider for the  $\beta$ -phase film when compared to those for the  $\alpha$ -phase one. This is because a smaller value range tends to provide a larger deviation after normalization. From fitting the TR-PL spectra with Eq. (1), we obtained the  $\tau_{\text{avg}}$  of 17.7 ns for the  $\alpha$ -phase film, whereas we obtained that of 2.7 ns for the  $\beta$ -phase one. Thus, the  $\tau_{\text{avg}}$  of the  $\beta$ -phase is shorter by 1/6–1/7 times than that of the  $\alpha$ -phase. This indicates that the excitons generated in the  $\beta$ -phase film were immediately recombined to disappear. Specifically, although a large number of excitons were generated due to the intense optical absorbance of the  $\beta$ -phase film, most of them were immediately annihilated via radiative relaxation. We next consider the reason behind the short PL lifetime of the  $\beta$ -phase film. As shown in Figs. 1(b) and 1(c) [or Fig. 4(b)], the  $\beta$ -phase has a herringbone-type arrangement assembled by tilted-stacking ZnPc planar molecules, where the individual stacked ZnPc chains are discontinuously connected adjacent to each other unlike that for the brickstone-type  $\alpha$ -phase. This implies that excitons are hard to move to adjacent stacking chains, and thus, the annihilation of excitons easily takes place to reduce the lifetime for the  $\beta$ -phase structure.

Considering that the  $\alpha$ - and  $\beta$ -phase ZnPc films are used as a donor for OPVs, they have some advantages and disadvantages by judging from the above findings. For the  $\beta$ -phase film, the molecular-scale flatness and well-ordered arrangements are advantageous to fabricate well-controlled D/A interfaces for OPVs, which certainly contribute to reproduce the device performance. Since the optical absorbance of the  $\beta$ -phase ZnPc film is greater by 1.5–2 times than that of the  $\alpha$ -phase ZnPc film in the UV-vis-NIR range, the number of excitons generated in the  $\beta$ -phase film is approximated to be increased by 1.5–2 times when compared to that in the  $\alpha$ -phase film. However, the  $\tau_{\text{avg}}$  of the excitons for the  $\beta$ -phase film is shorter by 1/6–1/7 times than that for the  $\alpha$ -phase one. This suggests that the number of excitons separating to electrons and holes at the D/A interface is reduced by the corresponding orders. On the contrary, for the  $\alpha$ -phase film, the number of excitons contributing to photocurrent is expected to be larger by 6–7 times than that for the  $\beta$ -phase one, although the number of photogenerated excitons is smaller by 1/2–2/3 times than that for the  $\beta$ -phase. Furthermore, although the surface of the  $\alpha$ -phase film is rougher than that of the  $\beta$ -phase one and thus the D/A interface cannot be well defined, the D/A interface area becomes rather large as a result and it may play a role in increasing the number of carriers at the interface.

Judging comprehensively from the discussion above, the  $\alpha$ -phase film seems to be superior to the  $\beta$ -phase one as a donor used for OPVs. To confirm this assumption, we actually fabricated [ITO/ $\alpha$ -ZnPc/C<sub>60</sub>/Al] and [ITO/ $\beta$ -ZnPc/C<sub>60</sub>/Al] OPV cells and measured their EQE with respect to a wavelength ( $\lambda$ ) of light by electric-field modulated spectroscopy.<sup>5,8</sup> Figure 8 shows the

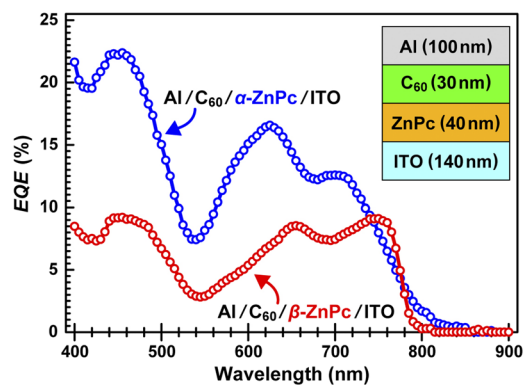


**FIG. 8.** Comparison in EQE between [ITO/α-ZnPc/C<sub>60</sub>/Al] (blue) and [ITO/β-ZnPc/C<sub>60</sub>/Al] (red) OPV cells. Inset schematically illustrates the OPV cell structure using the  $\alpha$ - and  $\beta$ -phase ZnPc films as a donor.

EQE- $\lambda$  plot for the two OPV cells. The inset schematically illustrates the OPV cell structure. As expected above, [ITO/α-ZnPc/C<sub>60</sub>/Al] OPV exhibits a larger EQE by ~2 times than that for [ITO/β-ZnPc/C<sub>60</sub>/Al] OPV in the range of 400 nm–700 nm. This suggests that not only larger optical absorbance but also longer exciton lifetime are the important factors to improve EQE of OPVs.

#### IV. SUMMARY

We have examined the structural and optical properties of the  $\alpha$ - and  $\beta$ -phase ZnPc films from a viewpoint of application to OPVs. The FT-IR results suggest that the brickstone arrangement was dominant for the  $\alpha$ -phase. When the  $\alpha$ -phase was transited to the  $\beta$ -phase, the structural and optical properties were correspondingly changed: (i) the size of crystalline grains drastically increased along a lateral direction to substrate and a continuous and molecular-level flat surface of ZnPc films was formed, (ii) the optical absorbance became greater by 1.5–2 times in UV-vis-NIR range, and (iii) the average exciton lifetime became shorter by 1/6–1/7 times. We fabricated OPVs using the  $\alpha$ - and  $\beta$ -phase ZnPc films as a donor and found that the OPV using the  $\alpha$ -phase film exhibited an external quantum efficiency larger by ~2 times than OPV using the  $\beta$ -phase film in the wavelength range of 400 nm–700 nm. The findings obtained in the present study suggest that it is important to design and synthesize a donor film exhibiting simultaneously not only a larger optical absorbance but also a longer exciton lifetime for development of high performance OPVs.

#### ACKNOWLEDGMENTS

We are grateful to Dr. S. Kawano and Professor K. Tanaka at Nagoya University for AFM measurements. We are also thankful to Venture Business Laboratory of Nagoya University for XRD experiments. The present work was partially supported by the Japan-France Research Cooperative Program between the JSPS (Japan Society for the Promotion of Science) and CNRS (Center National de la Recherche Scientifique).

## DATA AVAILABILITY

The data that support the findings of this study are available from the corresponding author upon reasonable request.

## REFERENCES

- <sup>1</sup>For example: *Organic Solar Cells: Materials, Devices, Interfaces, and Modeling*, edited by Q. Qiao (CRC Press, New York, 2015).
- <sup>2</sup>P. Peumans, A. Yakimov, and S. R. Forrest, *J. Appl. Phys.* **93**, 3693 (2003).
- <sup>3</sup>M. C. Scharber and N. S. Sariciftci, *Prog. Polym. Sci.* **38**, 1929 (2013).
- <sup>4</sup>A. Slaoui and R. T. Collins, *MRS Bull.* **32**, 211 (2007).
- <sup>5</sup>S. Ryuzaki and J. Onoe, *Nano Rev.* **4**, 21055 (2013).
- <sup>6</sup>S. Günes, H. Neugebauer, and N. S. Sariciftci, *Chem. Rev.* **107**, 1324 (2007).
- <sup>7</sup>Y. Liang, Z. Xu, J. Xia, S.-T. Tsai, Y. Wu, G. Li, C. Ray, and L. Yu, *Adv. Mater.* **22**, E135 (2010).
- <sup>8</sup>S. Ryuzaki and J. Onoe, *J. Phys. D: Appl. Phys.* **44**, 265102 (2011).
- <sup>9</sup>S. Ryuzaki, T. Kai, Y. Toda, S. Adachi, and J. Onoe, *J. Phys. D: Appl. Phys.* **44**, 145103 (2011).
- <sup>10</sup>S. Ryuzaki and J. Onoe, *Jpn. J. Appl. Phys., Part 1* **52**, 06GD03 (2013).
- <sup>11</sup>Y. Zhou, T. Taima, T. Miyadera, T. Yamanari, and Y. Yoshida, *J. Appl. Phys.* **111**, 103117 (2012).
- <sup>12</sup>S. Heutz, S. M. Bayliss, R. L. Middleton, G. Rumbles, and T. S. Jones, *J. Phys. Chem. B* **104**, 7124 (2000).
- <sup>13</sup>A. A. Zanfolim, D. Volpati, C. A. Olivati, A. E. Job, and C. J. L. Constantino, *J. Phys. Chem. C* **114**, 12290 (2010).
- <sup>14</sup>M. M. El-Nahass, H. M. Zeyada, M. S. Aziz, and N. A. El-Ghamaz, *Opt. Mater.* **27**, 491 (2004).
- <sup>15</sup>S. Senthilarasu, Y. B. Hahn, and S.-H. Lee, *J. Appl. Phys.* **102**, 043512 (2007).
- <sup>16</sup>L. Gaffo, M. R. Cordeiro, A. R. Freitas, W. C. Moreira, E. M. Girotto, and V. Zucolotto, *J. Mater. Sci.* **45**, 1366 (2010).
- <sup>17</sup>S. Schäfer, A. Petersen, T. A. Wagner, R. Kniprath, D. Lingenfelser, A. Zen, T. Kirchartz, B. Zimmermann, U. Würfel, X. Feng, and T. Mayer, *Phys. Rev. B* **83**, 165311 (2011).
- <sup>18</sup>B. Verreet, P. E. Malinowski, B. Niesen, D. Cheyns, P. Heremans, A. Stesmans, and B. P. Rand, *Appl. Phys. Lett.* **102**, 043301 (2013).
- <sup>19</sup>B. P. Rand, D. Cheyns, K. Vasseur, N. C. Giebink, S. Mothy, Y. Yi, V. Coropceanu, D. Beljonne, J. Cornil, J.-L. Brédas, and J. Genoe, *Adv. Funct. Mater.* **22**, 2987 (2012).
- <sup>20</sup>T.-M. Kim, J. W. Kim, H.-S. Shim, and J.-J. Kim, *Appl. Phys. Lett.* **101**, 113301 (2012).
- <sup>21</sup>Z. Wang, T. Miyadera, A. Saeki, Y. Zhou, S. Seki, Y. Shibata, T. Yamanari, K. Matsubara, and Y. Yoshida, *J. Appl. Phys.* **116**, 013105 (2014).
- <sup>22</sup>M. K. Debe and D. R. Field, *J. Vac. Sci. Technol., A* **9**, 1265 (1991).
- <sup>23</sup>F. H. Moser and A. L. Thomas, *Phthalocyanine Compounds*, ACS Monograph Series Vol. 157 (ACS, New York, 1963).
- <sup>24</sup>A. C. Cruickshank, C. J. Dotzler, S. Din, S. Heutz, M. F. Toney, and M. P. Ryan, *J. Am. Chem. Soc.* **134**, 14302 (2012).
- <sup>25</sup>J. Onoe and K. Takeuchi, *Phys. Rev. B* **54**, 6167 (1996).
- <sup>26</sup>K. Tateishi, M. Funato, Y. Kawakami, K. Okamoto, and K. Tamada, *Appl. Phys. Lett.* **106**, 121112 (2015).
- <sup>27</sup>K. Ogasawara, T. Iwata, Y. Koyama, T. Ishii, I. Tanaka, and H. Adachi, *Phys. Rev. B* **64**, 115413 (2001).
- <sup>28</sup>S. Watanabe, K. Ogasawara, M. Yoshino, and T. Nagasaki, *Phys. Rev. B* **81**, 125128 (2010).
- <sup>29</sup>M. Gouterman, *J. Chem. Phys.* **30**, 1139 (1959).
- <sup>30</sup>M. Gouterman, *J. Mol. Spectrosc.* **6**, 138 (1961).
- <sup>31</sup>M. Gouterman, D. Holten, and E. Lieberman, *Chem. Phys.* **25**, 139 (1977).
- <sup>32</sup>Y. Yoon, S. Kim, and H. C. Choi, *NPG Asia Mater.* **12**, 16 (2020).
- <sup>33</sup>D. R. Tackley, G. Dent, and W. E. Smith, *Phys. Chem. Chem. Phys.* **2**, 3949 (2000).
- <sup>34</sup>J. S. Louis, D. Lehmann, M. Friedrich, and D. R. T. Zahn, *J. Appl. Phys.* **101**, 013503 (2007).
- <sup>35</sup>N. Uyeda, M. Ashida, and E. Suito, *J. Appl. Phys.* **36**, 1453 (1965).
- <sup>36</sup>M. Ashida, N. Uyeda, and E. Suito, *Bull. Chem. Soc. Jpn.* **39**, 2616 (1966).
- <sup>37</sup>F. Iwatsu, *J. Phys. Chem.* **92**, 1678 (1988).
- <sup>38</sup>E. A. Ough, M. J. Stillman, and K. A. M. Creber, *Can. J. Chem.* **71**, 1898 (1993).
- <sup>39</sup>S. Karan and B. Mallik, *J. Phys. Chem. C* **111**, 7352 (2007).
- <sup>40</sup>D. Yokoyama, Z. Q. Wang, Y.-J. Pu, K. Kobayashi, J. Kido, and Z. Hong, *Sol. Energy Mater. Sol. Cells* **98**, 472 (2012).
- <sup>41</sup>Y. Zhou, T. Taima, T. Miyadera, T. Yamanari, M. Kitamura, K. Nakatsu, and Y. Yoshida, *Nano Lett.* **12**, 4146 (2012).
- <sup>42</sup>B. Yu, L. Huang, H. Wang, and D. Yan, *Adv. Mater.* **22**, 1017 (2010).
- <sup>43</sup>J. Onoe, S. Watanabe, S. Kato, M. Nakaya, and J.-P. Bucher, *J. Chem. Phys.* **147**, 214701 (2017).
- <sup>44</sup>T. C. Van Cott, J. L. Rose, G. C. Misener, B. E. Williamson, A. E. Schrimpf, M. E. Boyle, and P. N. Schatz, *J. Phys. Chem.* **93**, 2999 (1989).
- <sup>45</sup>G. A. Peralta, M. Seth, and T. Ziegler, *Inorg. Chem.* **46**, 9111 (2007).
- <sup>46</sup>M. Guo, R. He, Y. Dai, W. Shen, M. Li, C. Zhu, and S. H. Lin, *J. Chem. Phys.* **136**, 144313 (2012).